Modeling of cavitation in hydraulic turbomachinery

Ridha Zgolli, Marwa Ennouri, Hatem Kanfoudi

Modeling of cavitation in hydraulic turbomachinery

Ridha Zgollli[1]*, Marwa Ennouri [2], Hatem Kanfoudi[3]

ISROMAC 2016

International Symposium on Transport Phenomena and Dynamics of Rotating Machinery

Hawaii, Honolulu

April 10-15, 2016

Abstract

This paper aligns itself to many other research developments concerning hydrodynamic cavitation. It attempts to provide an increasingly reliable tool for the analysis and control of particular flows in a hydraulic turbomachinery. This paper consists of two parts. The first one deal with the basic investigations of cavitating flow around an inclined two-dimensional profile using a recently developed and validate cavitation model. The second part describes the application of this model to predict the head drop behaviour of a centrifugal pump. A 3D numerical model is proposed to simulate steady and unsteady internal flow into a centrifugal pump with both, non-cavitating and cavitating operating conditions.We present the numerical approach and results, showing the ability to analyze the unsteady behavior of the internal flow related to the rotation of the wheel induced by the passage of the blades front the volute beak.

Keywords

Turbomachinery —Cavitation — CFD

[1]*Department of Civil Engineering, University of Tunis El Manar, Tunis, Tunisia*

[2]*Department of Civil Engineering, University of Tunis El Manar, Tunis, Tunisia*

[3]*Department of Civil Engineering, University of Tunis El Manar, Tunis, Tunisia*

*__Corresponding author__: Ridha.zgolli@enit.rnu.tn

INTRODUCTION

Cavitation generally occurs when the pressure in a certain region of liquid flow drops below the vapor pressure and, consequently, the liquid is vaporized and filled with cavity. Usually observed in various propulsion systems and high-speed underwater objects, such as marine propellers and hydraulic turbomachinery, this phenomenon causes severe noise, vibration and erosion [1].

Cavitation damage can be very expensive, and very difficult to eliminate. For most designers of hydraulic machinery, it is the preeminent problem associated with cavitation [2]. Therefore, to design a pump with high performance, a reliable prediction of this phenomenon is necessary. For this purpose, a new cavitation model based on the void fraction transport equation solved with the source term evaluating vaporization and condensation processes, has been integrated in the CFD-Code CFX developed at the Hydraulic and Environment Modeling Laboratory [MHE]. The Reynolds-averaged Navier-Stokes equations are solved for the mixture of liquid and vapor, which is considered as a single fluid with variable density. Variable density is expressed in terms of the volume fraction of the vapor phase. The closure of this variable is provided by the transport equation with our source term. This numerical model is used to calculate steady cavitating flow in pump Nsq 32. We have evaluated the cavitation performance of the pump, the distributions of the liquid pressure and the void fraction. The numerical results are also compared to ones obtained by the CFX cavitation model.

1. NUMERICAL ANALYSIS

Model and grid

The pump used in this study, has been the subject of previous experimental [3] and numerical [2] works. It is a centrifugal pump with specific speed of 32 ($n_{sq}32$). The main pump parameters and geometry are presented in table 1.The nominal operation is detected in the speed of rotation N = 1470 rev/min with a volumetric flow rate (water) Q_n = 590 m^3/h and and Hmt = 49m.

Table1. Geometrical parameters of the pump $n_{sq}32$

Parameters	value	Description
Impeller		
Ri	115mm	Inlet flange radius
R1	75mm	Mean impeller inlet radius
b1	85.9mm	Inlet impeller width
β1	70°	Inlet blade angle
θ1	37°	Blade LE inclination angle
R2	204.2mm	Mean impeller outlet radius
b2	42mm	Outlet impeller width
β2	63°	Outlet blade angle
θ2	90°	Blade Te inclination angle
Na	5	Blade number
e	8mm	Blade thickness
Volute		
R3	218mm	Base volute radius
b3	20mm	Volute width
φ_{outlet}	200mm	Outlet flange diameter

The first task to accomplish, on a numerical flow simulation is the definition of the geometry, followed by the grid generation. For the numerical simulation, an unstructured

mesh for the volute is used, whereas a structured mesh for the impeller and the inlet pipe was applied. Figure 1 shows the mesh of the impeller, the volute section and the entire computational domain.

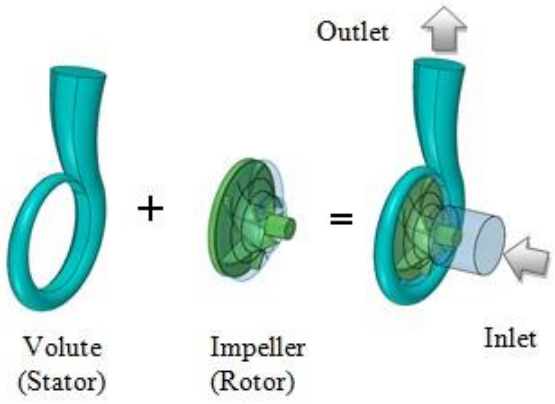

Figure 1. 3D elements of the pump Nsq 32

Numerical method

Governing equations ;

$$\frac{\partial \rho_m}{\partial t} + \frac{\partial (\rho_m u_j)}{\partial x_j} = 0 \quad (1)$$

$$\frac{\partial (\rho_m u_i)}{\partial t} + \frac{\partial (\rho_m u_j u_i)}{\partial x_j} = -\frac{\partial p}{\partial x_i} + A + B \quad (2)$$

With

$$A = \frac{\partial}{\partial x_j}\left[(\mu_m + \mu_t)\left(\frac{\partial u_i}{\partial x_i} + \frac{\partial u_j}{\partial x_j}\right)\right]$$
$$B = -\rho_m \omega u_i + \rho_m \omega(\omega . r)$$

Coriolis forces and centrifugal forces are added as a dynamic source term (term B).

Simulation parameters and boundary conditions;

The general parameters and boundary conditions used for the 3D flow simulation of the pump are summarized in table 2. The rotating and stationary domains were connected by the General Grid Interface (**GGI**). The Frozen Rotor interface model was set for the steady simulation, which treats the flow from one component to the next by changing the frame of reference. The Transient Rotor-Stator interface model was set for the unsteady simulation, which takes into account of all the transient flow characteristics and allows a smooth rotation between components.

Table2. Impeller NS32: simulation parameters

Parameters	CFX
Flow simulation domain	Entire pump
Grid	Structured impeller, unstructured volute
Fluid	Water
Inlet	Static pressure=101 325 Pa
Outlet	Mass Flow =variable(kg/s)
Turbulence model	SST
Discretization	Second Order
Maximum residual convergence criteria	10^{-4}

2. CAVITATION MODEL [4]

Cavitation models in the literature, based on the same approach of flow for "homogeneous mixture" with a density ρ_m (eq.6), can be classified into two categories depending on the source term S_α assessment technique (second term in equation (5)). Some use a particular behavior law to translate the vapor phase presence effect [5], [6] and others [7], [8] are inspired by the dynamic behavior of the bubble governed by the Rayleigh-Plesset equation .In this second category that comes to rank the model used here [9], with source terme evaluated with equations (7), (8), (9), (10) and (11) . We note therefore that the character 'active' given to α rate remains dependent on the numerical scheme adopted by the used CFD solver code. Velocity interface $\dot{R}$ computed using integration of Rayleigh-Plesset equation with some assupmtions (ignoring the viscosity and surface tension effects) becomes;

$$\dot{R} = \pm\left|\left(\frac{2}{3}\frac{p_v - p_\infty}{\rho_l}\right)\left(1 - \frac{R_0^3}{R^3}\right)\right|^{\frac{1}{2}} \quad (3)$$

During evaporation of liquid; $\dot{R}$ is positive and we have $(1 - \frac{R_0^3}{R^3}) \approx 1$ and the right term of precedent relation can be evaluated correctly with equation (4);

$$\dot{R} = \sqrt{\frac{2}{3}(p_v - p_\infty)} \quad (4)$$

During the bubble collapse; when R approaching zero, the term $\frac{R_0^3}{R^3}$ becomes preponderant into equation (3) and it is evaluated here with the term $\Phi(\alpha)$ into equation (10)

$$\frac{\partial (\rho_v \alpha)}{\partial t} + \frac{\partial (\rho_v \alpha u_j)}{\partial x_j} = S_\alpha = \dot{m}^v + \dot{m}^c \quad (5)$$

$$\rho_m = \alpha \rho_v + (1 - \alpha)\rho_l \quad (6)$$

$$S_\alpha = C_{pd} f(\alpha) g(\alpha, p) sign\big(g(\alpha, p)\big) \quad (7)$$

With:

$$C_{pd} = \sqrt{6}\sqrt[3]{\frac{4}{3} n_0 \pi}\,\frac{\rho_v \rho_l}{\rho_m} \quad (8)$$

$$f(\alpha) = \alpha^{\frac{2}{3}}(1 - \alpha)^{\frac{4}{3}} \quad (9)$$

$$g(\alpha, p) = \left(\frac{p_v - p_\infty}{\rho_l}\right)(1 - \Phi(\alpha)) \quad (10)$$

$$\Phi(\alpha) = \frac{4 R_0 n_0 (1 - \alpha)}{\alpha} \quad (11)$$

More detail can be found in [9].

2D Unsteady cavitating flow

In all cases, the conventional condition for the appearance of cavitation is based on the pressure drop below the critical value pv (saturation vapor pressure) characteristic of the liquid in question for guiding the process of vaporization and condensation.
To validate the developed code, we present in Figure2 an experimental confrontation concerning obtained results for a flow around a cavitant NACA 0009 profile. It shows a comparison of the spectral analysis of the bearing capacity of the hydrofoil, between the experimental measurement [10] and the numerical result obtained by the proposed model. A good agreement can be noticed.

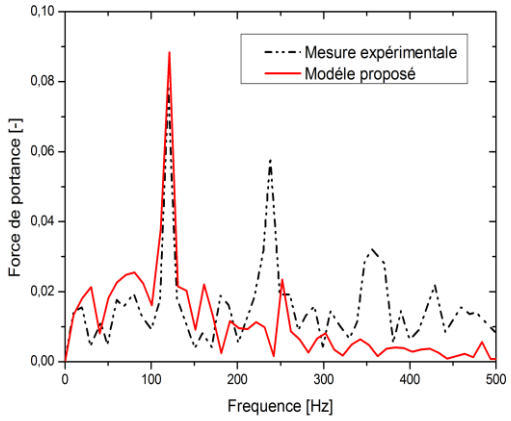

Figure 2. Comparison of the spectral analysis of the bearing capacity of the NACA 0009 profile (i=0°, σ=1.2**,** cycle frequency is 120 Hz, equivalent to a period T = 0.008s).

For performance evaluation of the used model, a 2D flow around a NACA 0009 hydrofoil is computed, taking into account the compatibility of the turbulence model. The simulations were carried out for an angle of incidence i=5°, and a cavitation number σ=1.2. Inflow velocity U_{ref}= 20m/s and a turbulence intensity of 1% were assumed.For the simulation of the cavitating flow around the hydrofoil a multi-block structured grid was used, see Figure 3.

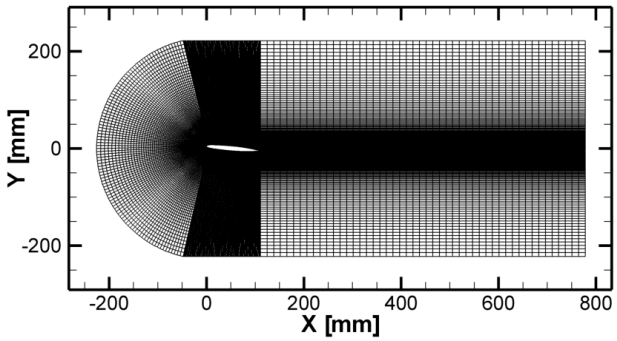

Figure 3. Multi-block grid topology for the simulation

The results presented in Figure 4 show that this model is able to control the re-entrant jet, following the evolution of unstable cavitation pockets. We observe vapor cavities convected by the flow from the previous cycle (0.1T), and then a new one expands at the leading edge. This is the growth phase (0.2T to 0.5T); it reaches its maximum length to 0.5T. Then, as the re-entrant jet reaches the high pressure gradient region (the pocket closure area), it becomes more important and begins to move upstream toward the leading edge along the surface of the hydrofoil below the vapor pocket (0.6T to 1T). It decomposes the main vapor pocket in small cavities that are then moved by the flow downstream (trailing edge), after which we are witnessing the start of a new cycle.

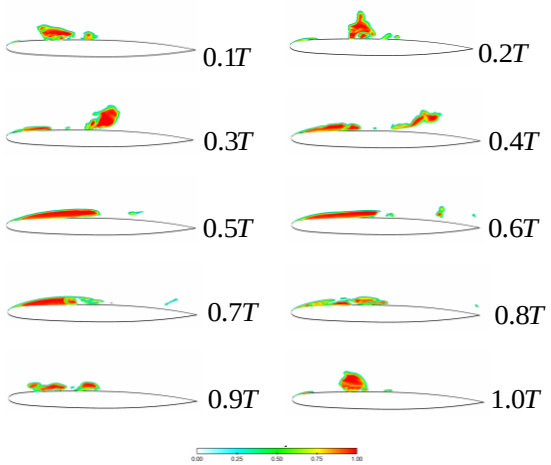

Figure 4. Evolution of α for a flow around a cavitating NACA09 profile (σ=1.2, incidence i=5°, T = 0.008s) [9].

3. FLOW THROUGH A CENTRIFUGAL PUMP

Non-Cavitating internal flow

For this study a SST model is adopted for steady flow. In fact, results using different turbulence models, led to the selection of the SST model that has proved satisfactory especially when it comes to part-flow operation. Figure 5 shows the performance of the pump compared with the experimental results [3] and the numerical analysis.The calculated and measured variables of the analyzed centrifugal pump are presented by means of the dimensionless coefficients, which are defined as follows:

Flow coefficient (ϕ):

$$\phi = \frac{Q}{(\omega . {d_2}^3)}$$

Head coefficient(Ψ):

$$\psi = \frac{g.H}{(\omega^2 . {d_2}^2)}$$

where Q, H, ω, d_2 and g refer to flow, total head, angular velocity, impeller outlet diameter and gravity respectively. We note that the total head was calculated by mass flow averaging.

The experimental results are higher than the numerical ones according to the decrease of the flow. This can be the consequence of excessive loss estimation. However, we notice that the shape of the curve presents the same tendency, with a maximal error of 11% over the entire flow. We can consider that the results of the numerical analysis are quite acceptable

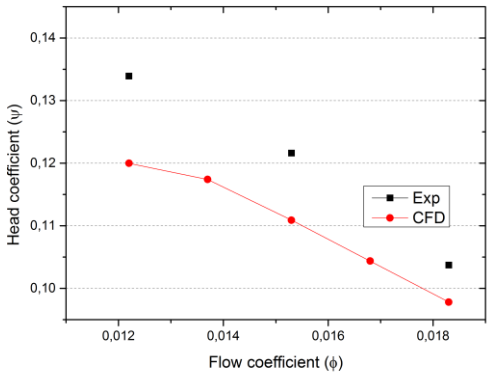

Figure 5. Performance curves of experimental results and numerical analysis for steady state simulation

A transient calculation was subsequently conducted with the SST model and using wide range of flow rates. We present some results (Figure 6) showing the fluctuations of the head coefficient for a simulation time covering two full revolution of the impeller.Fluctuations induced by the passage of each blade front the volute beak are clearly represented. We observe that they are greater for Qn, 1.1Qn and 1.2Qn as a direct consequence of the water transmission rate amplification. Figure7presents calculation results of the torque coefficient of the hydraulic forces applied to the movable wheel. As dimensionless coefficient, the torque coefficient (χ) is written as follows:

$$\chi = \frac{M}{\rho . \omega^2 . {d_2}^5} \quad (7)$$

With M,ω,d_2,ρ refer to Torque on the impeller shaft, angular velocity, impeller outlet diameter and water density respectively.

We notice that the reduction in torque fluctuations depends on the flow rate increases for a fixed speed (1470 rev / min). This result is explained by the fact that the increase in fluid flow rate through the wheel is accompanied by a pressure reduction.

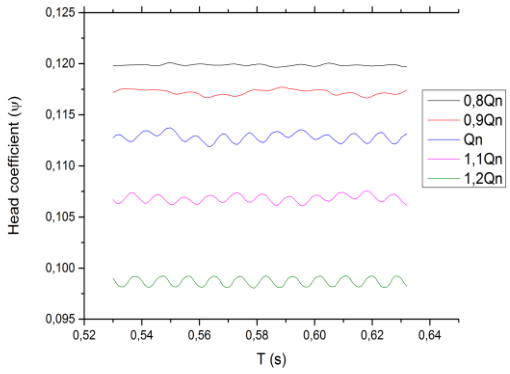

Figure 6. Head coefficient calculated for different flow rates

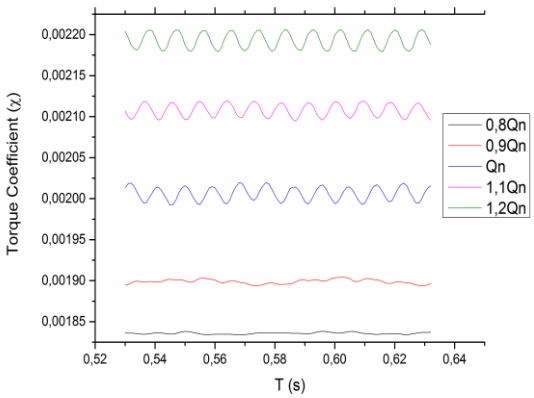

Figure 7. Torque coefficient applied to the rotor

Cavitating internal flow

For the simulation of the cavitating flow, unsteady calculations are very time consuming, so we will restrict ourselves to the stationary ones. But it should be noted that the transient calculations are underway for further future research.

In this section we will focus on the internal flow corresponding to the conditions of the occurrence of cavitation coupled to cavitation model presented above and the one implemented in the CFX code. To be clearer it should be known that the cavitation model built at Ansys CFX 15.0 is derived from a simplified Rayleith–Plesset equation that neglects the second-order derivative of the bubble radius with time and the bubble–bubble interaction [11].

First a stationary calculation at a high pressure level is performed to ensure non-cavitating conditions in the whole computational domain. Then the inflow pressure is lowered in small steps. During this process, vapor structures appear in the regions of low static pressure. The more the pressure level is lowered, the more the cavitation zone grows, influencing the impeller head [12].

The computations were carried out for several cavitation numbers starting from σ = 0.25. The cavitation number (σ) is defined as:

$$\sigma = \frac{NPSH}{H} \quad (8)$$

The NPSH value is outlined as the total pressure of the fluid at the inlet section above the vapor pressure p_v of the fluid depending on the fluid temperature T, divided by ρ.g:

$$NPSH = \frac{Pt_{in} - P_v}{\rho * g} \quad (9)$$

The head H is computed from the CFD simulation results by averaging the total pressure at the inlet Pt_{in} and the outlet Pt_{out} of the computational domain.

$$H = \frac{Pt_{out} - Pt_{in}}{\rho * g} \quad (10)$$

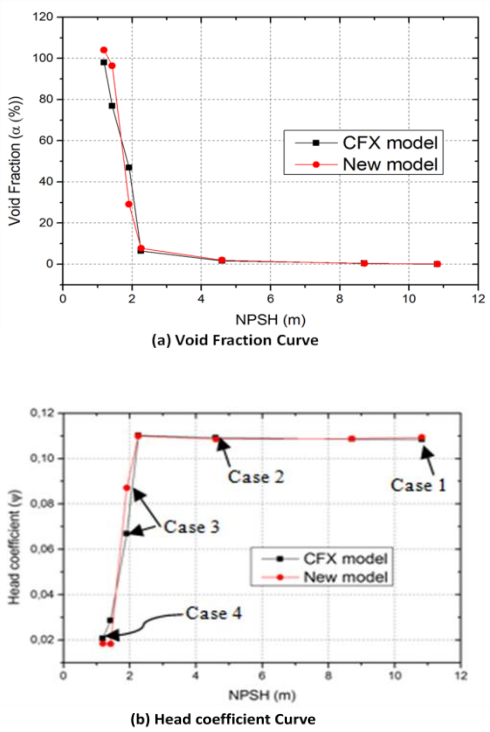

Figure 8. Cavitation performance of the centrifugal pump

Figure 8 shows a comparison between the calculated cavitation performance for the nominal flow rate for both the CFX and the new cavitation model. From the figure (b) Head coefficient Curve, we can notice that the new model head drop occurs almost at the same NPSH value as the CFX one. The two curves are very close and particularly confused view of NPSH= 10.83m to NPSH= 2.26m. From NPSH=2.26m the void fraction **α= (Vapor volume/Water volume)** predicted inside the Impeller by the new model is slightly higher than the CFX one except for NPSH=1.91m5(figure (a)). We can say that, generally, both two models behave the same way.

Figure 9 illustrate the numerical results of the void volume fraction distributions in Cases 1-4 in Fig. 8.b. In void volume fraction distributions, the red regions indicate the occurrence of the vapor. The cavitating region noticeably expands on the blade with a decrease in the NPSH. Therefore, we will consider the case 3 (NPSH 1.91m) corresponding to a vapor fraction with a value of 46.9% for CFX cavitation model and a vapor fraction of 29.1% for the proposed model, as the cavitating case.

CONCLUSION

A new cavitation model has been integrated in the Ansys CFX code. Unsteady simulations have been performed for cavitating flow around a hydrofoil. Based on these investigations, the cavitating flow through a centrifugal pump has been simulated in a good agreement with the results obtained from the CFX cavitation model.

The results of the unsteady simulation show the typical development of a re-entrant-jet and the evolution of unstable cavitation pockets.

Also the flow through a centrifugal pump NS32 has been simulated. The computed head-drop and the comparison of the behavior of the two cavitation models towards the occurrence of cavitation phenomenon indicate that both of them predict it correctly.

REFERENCES

[1] K. Dong-Hyun, P. Warn-Gyu and J. Chul-Min. Numerical simulation of cavitating flow past axisymmetric body. *Inter. J. Nav Archit Oc Engng*, 4: 256-266, 2012

[2] H. Lamloumi. Etude des modèles de cavitation-cas de référence et extension aux turbomachines hydrauliques. *Thèse de doctorat présentée à l'Ecole Nationale d'Ingénieurs de Tunis (ENIT)* ,2013

[3] M. Asuaje, F. Bakir, S. Kouidri, F. Kenyery and R. Rey. Numerical Modelization of the Flow in Centrifugal Pump: Volute Influence in Velocity and Pressure Fields. *Inter. J. of Rotating Machinery*,3 :244-255, 2005

[4] H. Kanfoudi. Modélisation de la cavitation dans un écoulement turbulent *Thèse de doctorat présentée à l'Ecole Nationale d'Ingénieurs de Tunis (ENIT)*, 2012

[5] A. K. Singhal, M. M. Athavale, H. Li and Y. Jiang. Mathematical basis and validation of the full cavitation model. *J. of Fluids Engineering* 124:617- 624, 2000

[6] J. L. Reboud, B. Stutz, and O. Coutier. Two-phase flow structure of cavitation: experiment and modeling of unsteady effect. *Third Inter .Symp. on Cavitation (Grenoble, France)*, 1998

[7] W. Yuan, J. Sauer and G. H. Schnerr . Modeling and computation of unsteady cavitation flows in injection nozzles. *Mec. Ind*, 383-394, 2001

[8] Y. Delannoy and J.L. Kueny. Two-Phase Flow Approach in Unsteady Cavitation Modeling. *Cavitation and multiphase flow forum.*153–158, 1990

[9] H. Kanfoudi and R . Zgolli. A Numerical model to simulate the cavitating flows. *Int. J. of Modeling Simulation and Scientific Computing,* 2 :277-297, 2010

[10] Y. Ait Bouziad. Physical modelling of leading edge cavitation: computational methodologies and application to hydraulic machinery .*Thèse de doctorat présentée à l' EPFL- Lausanne*, 2006

[11] P . ZwarT, A. Gerber and T. Belamri. A two-phase flow model for predicting cavitation dynamics. *Proc of the Fifth Inter Conf on Multiphase Flow (Yokohama, Japan),* 2004

[12] M. Frobenius and R. Schilling. Cavitation prediction in hydraulic machinery. *22nd Symp on Hydraulic Machinery and Systems (Stockholm,Sweden*), 2004

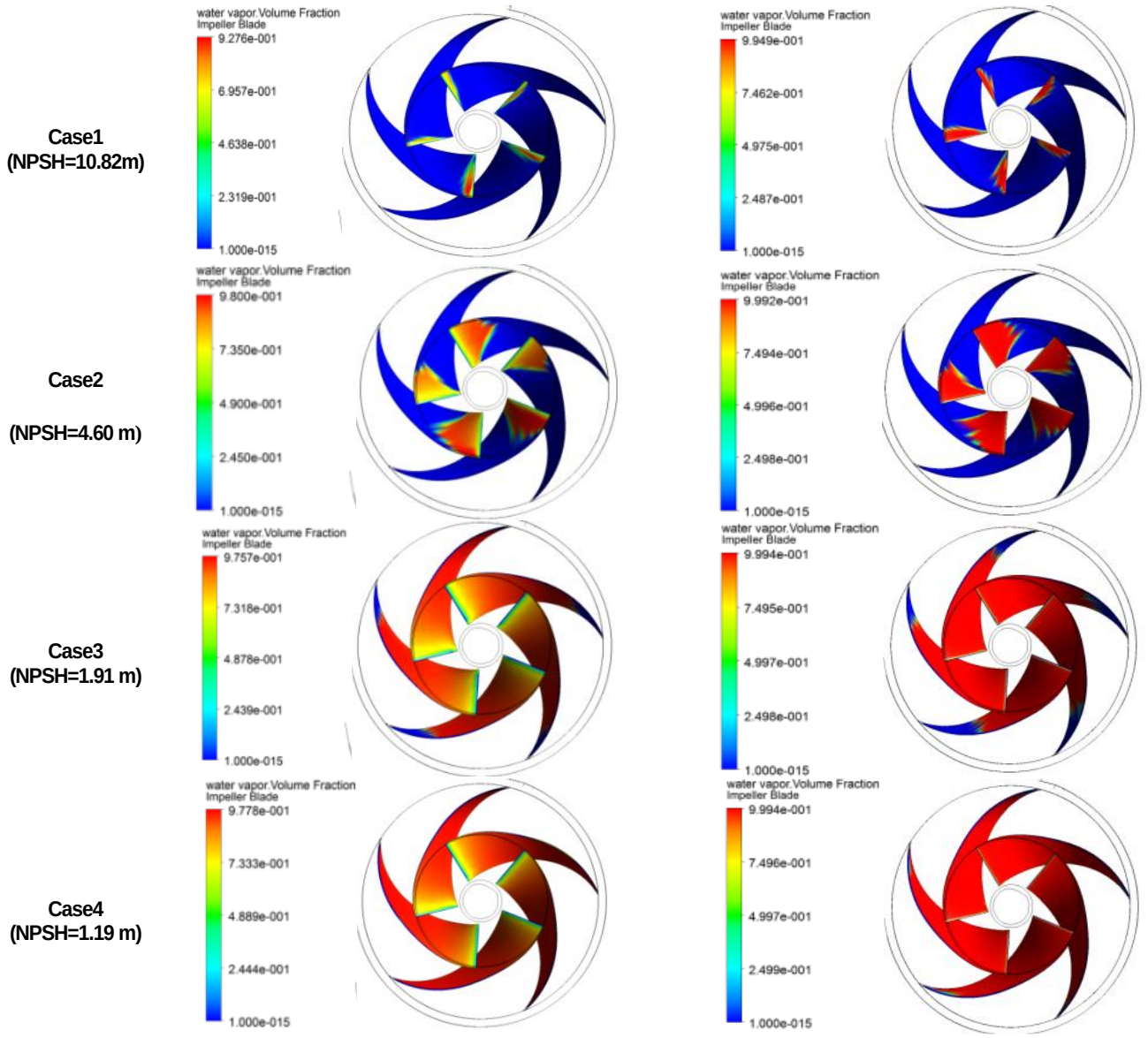

(a) Void volume fraction (CFX model) (b) Void volume Fraction (New model)

Figure 9. Predicted Void volume fraction distributions for the nominal flow rate Q_n